Magneto-structural instability in $Ni_2Mn_{1.4}Sb_{0.6}$ alloy

2007 J. Phys.: Condens. Matter 19 346213

(http://iopscience.iop.org/0953-8984/19/34/346213)

J. Phys.: Condens. Matter **19** (2007) 346213 (10pp) doi:10.1088/0953-8984/19/34/346213

Magneto-structural instability in $Ni_2Mn_{1.4}Sb_{0.6}$ alloy

S Chatterjee[1], S Giri[1], S Majumdar[1], A K Deb[2], S K De[2] and V Hardy[3]

[1] Department of Solid State Physics, Indian Association for the Cultivation of Science, 2A & B Raja S C Mullick Road, Kolkata 700 032, India
[2] Department of Materials Science, Indian Association for the Cultivation of Science, 2A & B Raja S C Mullick Road, Kolkata 700 032, India
[3] Laboratoire CRISMAT, ENSICAEN, 6 Boulevard du Marechal Juin, 14050 Caen Cedex, France

E-mail: sspsm2@iacs.res.in (S Majumdar)

Received 7 May 2007, in final form 7 June 2007
Published 24 July 2007
Online at stacks.iop.org/JPhysCM/19/346213

Abstract

We present here a detailed investigation of the magnetic and structural behaviours of a ferromagnetic shape memory alloy with nominal composition $Ni_2Mn_{1.44}Sb_{0.6}$. The alloy undergoes a structural transition from a high-temperature cubic phase ($Fm\bar{3}m$) to an orthorhombic low-temperature phase below approximately 200 K. We observe a clear signature of this martensitic transformation in resistivity, magnetic susceptibility, heat capacity and x-ray diffraction data. The first-order nature of the transition is clear from the thermal irreversibility present in the temperature dependence of various physical properties. A wide region of phase coexistence across the martensitic transformation, arising from the influence of disorder on the first-order phase transition, is observed. A small but positive entropy change due to an applied magnetic field occurs across the region of phase coexistence. An interplay between the structural and magnetic behaviour is evident from our study.

1. Introduction

Ferromagnetic shape memory alloys (FSMAs) are materials which exhibit both shape memory effect and ferromagnetism. There have been considerable interest in the field of FSMAs triggered by the discovery of large magnetic-field-induced strain in Ni_2MnGa-based alloys [1]. In some non-stoichiometric alloys of Ni_2MnGa, as large as 9% strain is observed at an applied field of 10 kOe [2]. FSMAs enjoy the advantage as smart materials over conventional shape memory alloys because, in the absence of any thermal-related mechanism, the response is much faster. Shape memory alloys are all associated with a first-order diffusionless structural phase transition, called the martensitic transition (MT) [3]. The martensitic phase develops with some spatially inhomogeneous substructure, known as martensite variants. The interfaces between the martensite variants are mobile. The obvious mechanism for the field-induced strain is the rearrangements of martensite variants under an applied magnetic field (H). This is possible when the magneto-crystalline anisotropy energy is larger than the elastic energy involved in

the rearrangement of variants. Due to the lower point symmetry in the martensitic phase, the magnetic anisotropy is generally high, which favours large field-induced strain. The second mechanism that creates strain in FSMAs is the *field-induced MT*, where the external magnetic field triggers the structural transition. The largest possible strain in FSMAs, like Ni_2MnGa-based alloys, is observed near the MT, and therefore the ferromagnetic (FM) Curie temperature should be higher than the MT in the case of FSMAs.

Although the Ni–Mn–Ga system is a very promising candidate for FSMAs, there are a few other Mn-containing Heusler alloys, which show large magnetic-field-induced strain. Recently, the Ga-free $Ni_{50}Mn_{50-y}X_y$ (X = In, Sn and Sb) series of alloys has been found to exhibit a magnetic shape memory effect at considerably high temperature (close to room temperature) [4]. The martensitic and the magnetic transition temperatures vary widely with y (the extent of doping). For the X = Sn alloys, x-ray diffraction (XRD) and neutron diffraction have established that the MT takes place from the cubic $L2_1$ structure ($Fm\bar{3}m$) to an orthorhombic four-layered (4O) structure ($Pmma$) [5, 6].

The structural and magnetic transitions and their mutual correspondence in FSMAs is an intriguing phenomenon. While the MT is a first-order transition, the ferromagnetic transition is a second-order one. In these inherently disordered alloys, phase coexistence is observed across the MT, which is often termed as a *disordered influenced first-order phase transition* [7]. It is therefore important to know the effect of the MT on the ferromagnetic state of the system and vice versa. In the present work, we have investigated the Sb-based alloy with composition $Ni_2Mn_{1.4}Sb_{0.6}$ (this is equivalent to $Ni_{50}Mn_{35}Sb_{15}$ of [4]), which has a ferromagnetic T_C above room temperature; the MT occurs around 200 K. This provides us with an opportunity to investigate the structural transition, phase coexistence and magnetic behaviour over a wide temperature range through transport, magnetic, structural and heat capacity measurements. The investigations depict an anomaly in various physical parameters close to the structural transition, and also indicate a close inter-correlation between the magnetic and the structural behaviour of the material. A comparison with the Sn- and In-based compound, having similar composition to $Ni_2Mn_{1.4}Sb_{0.6}$, furnishes notable facts regarding the MT of these alloys.

2. Experimental details

The polycrystalline sample of $Ni_2Mn_{1.4}Sb_{0.6}$ was prepared by arc melting the constituent elements in argon atmosphere. The ingot was homogenized at 900 °C for 40 h, followed by a quenching in ice water. XRD patterns of the sample, both at room temperature and at different desired low temperatures, were taken with an X'Pert PRO diffractometer. The lattice parameter for the cubic $L2_1$ phase at room temperature was found to be $a = 5.99$ Å. The composition of the Ni–Mn–Sb alloy was checked by energy dispersive x-ray spectroscopy (EDS). The resistivity (ρ) of the sample was measured by the standard four-probe method in the temperature (T) range 10–300 K in a closed-cycle refrigerator (Janis Inc.). The magnetization (M) was measured using a commercial Quantum Design magnetic properties measurement system (MPMS) XL (Ever Cool model). The zero-field heat capacity (C_p) was measured by a relaxation technique using a commercial Quantum Design physical properties measurement system (PPMS).

3. Results

3.1. Transport

The inset of figure 1 shows the variation of ρ with T, which is associated with a clear anomaly due to the MT around 175 K: during heating there is a sharp fall in the ρ value around 150 K,

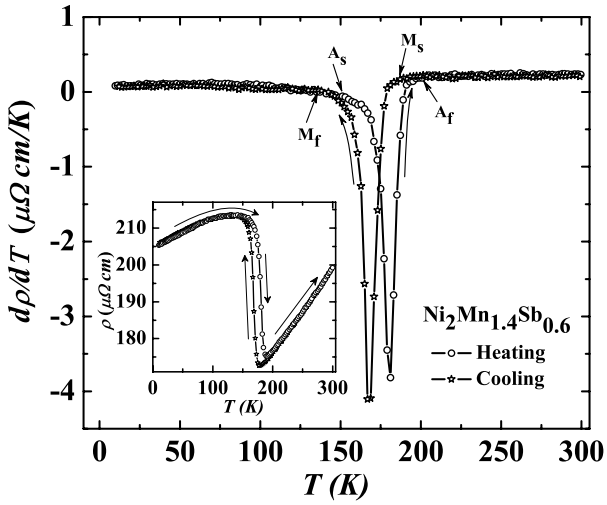

Figure 1. The temperature derivative of electrical resistivity ($d\rho/dT$) of $Ni_2Mn_{1.4}Sb_{0.6}$ is plotted against temperature (T). The inset shows the variation of resistivity with temperature both during heating and cooling.

while ρ shows a sharp rise around 170 K during cooling. The observed thermal hysteresis between 135 and 205 K indicates the first-order nature of the MT. From the positive value of the temperature derivative curve shown in figure 1, it is clear that the sample is metallic outside the region of thermal irreversibility. While cooling, the martensite grows between the temperatures M_s and M_f, and similarly the austenite grows between the temperatures A_s and A_f in the heating cycle (marked in figure 1). M_f and A_f can be identified as the two end points of the thermal hysteresis loop, while M_s and A_s are the points where $d\rho/dT$ starts to change during cooling and heating respectively. From the $d\rho/dT$ versus T graph, we found $M_s = 185$ K, $M_f = 135$ K, $A_s = 145$ K and $A_f = 205$ K. The observed transition temperatures are consistent with the previously reported values for this composition [4].

3.2. Temperature-dependent x-ray diffraction

Figure 2 shows the XRD pattern of $Ni_2Mn_{1.4}Sb_{0.6}$ for $40^\circ \leqslant 2\theta \leqslant 46^\circ$ at several temperatures during cooling and heating. The XRD patterns at 300 and 96 K for the full 2θ range of measurement are shown in figure 3(a). The room-temperature (300 K) data indicate that the sample has cubic $L2_1$ structure. As the sample is cooled down, a change in the diffraction pattern is observed. The $L2_1$ structure in the Ni–Mn–Sn Heusler system undergoes a martensitic transformation into an orthorhombic four-layered (4O) structure [4]. Recent results of neutron diffraction measurements by Brown *et al* suggest that the space group of the 4O structure is *Pmma* [6]. We are able to index all low-T peaks assuming an orthorhombic 4O structure in the region $15 \leqslant 2\theta \leqslant 90$ (see figure 3(a)), and the low-T crystal structure of $Ni_2Mn_{1.4}Sb_{0.6}$ is found to be identical with that of the Sn-based alloy of composition $Ni_2Mn_{1.44}Sn_{0.56}$.

Now let us look at the temperature evolution of the peaks in a restricted 2θ range as depicted in figure 2. The cubic and orthorhombic reflections are separately indexed with subscripts C and O, respectively. In the cooling leg (left panel of figure 2) of our data, we observe that the orthorhombic (221) Bragg peak first appears at $T = 207$ K. On further cooling

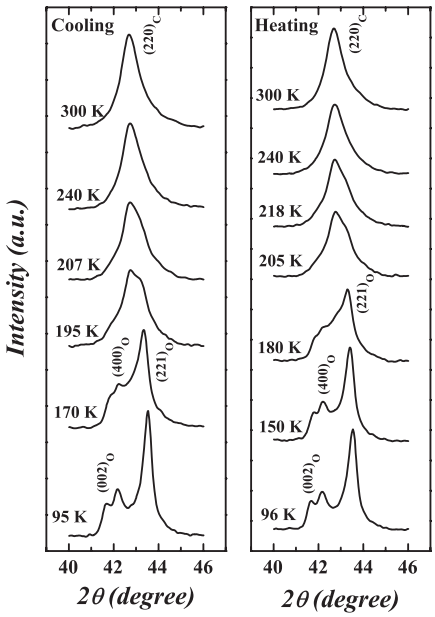

Figure 2. X-ray powder diffraction pattern of $Ni_2Mn_{1.4}Sb_{0.6}$ at various temperatures for both cooling and heating legs in a restricted range of 2θ (40°–46°). All the patterns are plotted in the same intensity scale for a comparison. The suffices C and O are for cubic and orthorhombic phases, respectively.

we observe that the intensities of the (002),(400) and (221) peaks increases. On the other hand, the peak intensity of the cubic (220) peak decreases with decreasing temperature. At 95 K, the orthorhombic peaks attain a reasonable intensity; however, the (220) cubic line is still present, which indicates that the transition is not complete even at 95 K. This is consistent with the magnetic susceptibility data (discussed below) where thermal hysteresis is present even below 95 K. The right panel of figure 2 shows the diffraction pattern during heating from 95 K, where the austenite phase develops from the martensite phase. The heating and cooling data are found to be different across the transition, which indicates the presence of thermal irreversibility in the XRD pattern.

It is clear that, over a wide temperature range, we observe a coexistence of both cubic (austenite) and orthorhombic (martensite) phases. In order to get a quantitative feeling of the coexisting phases across the MT, we have fitted the cubic and orthorhombic peaks with Lorentzian profiles for $40° \leqslant 2\theta \leqslant 47°$. For the mixed phase, in this 2θ range, we observe four peaks, which are cubic (220) and orthorhombic (022), (400) and (221). A multiple Lorentzian peak fitting is used to take into account all these four peaks. The fitting is performed on the data taken at different temperatures; however, it is shown for 96 K only (figure 3(b)). The individual intensities of the peaks, obtained from the fitting, are shown by dotted lines. We have plotted the ratio of the integrated intensities of the orthorhombic (221) and cubic (220) lines as a function of T. This ratio is somewhat equivalent to the ratio of orthorhombic to cubic phases in the system. It is clear from figure 3(c) that the intensity ratio follows different paths during heating and cooling, which is due to the hysteretic nature of the transition. Figure 3(d) shows the temperature dependence of lattice parameters in both the cubic and orthorhombic phases. Here the parameters (a_C) and (a_O, b_O and c_O) indicate the lattice parameters of the cubic ($L2_1$) and orthorhombic (4O) system respectively. The shaded region in the plot indicates the region of

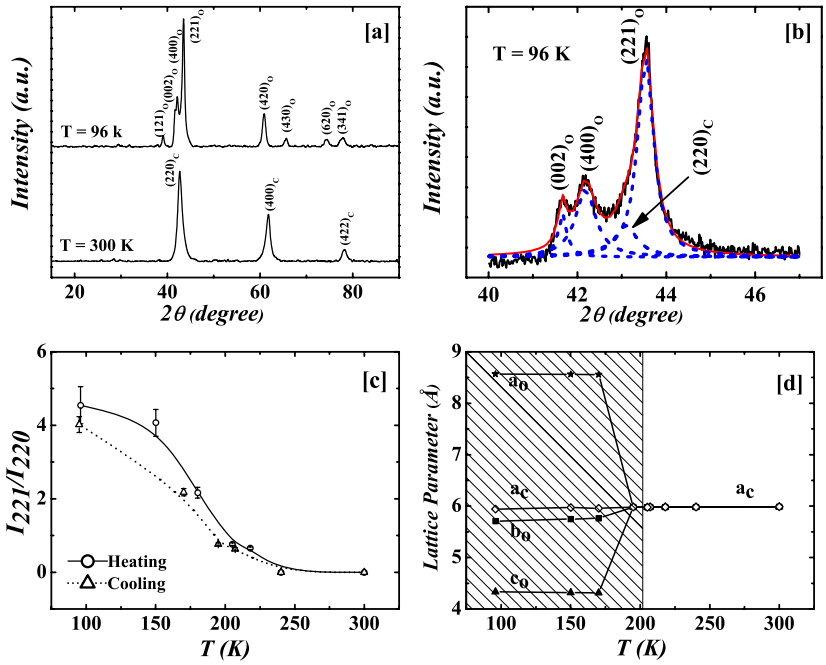

Figure 3. (a) X-ray diffraction patterns of the $Ni_2Mn_{1.4}Sb_{0.6}$ sample for the full 2θ range at 300 and 96 K. (b) Multiple Lorentzian profile fitting to the x-ray diffraction pattern in the 2θ range 40°–47° at $T = 96$ K, taking cubic and orthorhombic peaks into account. The dotted lines represent the individual peak intensities, while the solid line is the resultant intensity. (c) Ratio of the integrated intensities ($\frac{I_{221}}{I_{220}}$) of orthorhombic (221) and cubic (220) peaks as a function of temperature for $Ni_2Mn_{1.4}Sb_{0.6}$. (d) The variation of lattice parameters as a function of temperature. The shaded region signifies the region where both cubic and orthorhombic phases coexist. In all these plots, the suffices C and O denote cubic and orthorhombic peaks, respectively.

(This figure is in colour only in the electronic version)

phase coexistence. The lattice volume across the MT is found to remain almost constant. At 170 K, the orthorhombic lattice volume is 212.9 $Å^3$ (± 2), while the lattice volume in the cubic phase at 205 K is 213.9 $Å^3$ (± 2). Similar behaviour in lattice volume is observed in case of the Co_2NbSn Heusler compound [8].

3.3. Heat capacity

Figure 4(a) shows the variation of C_p of the $Ni_2Mn_{1.4}Sb_{0.6}$ alloy with temperature. There is a large anomaly observed at $T = 179$ K during warming the sample from 2.6 K, which is distributed over a very narrow temperature range of 5 K. This indicates the structural transition of the alloy from the martensite phase to the austenite phase and the sharp nature of the anomaly ensures the first-order nature of the transition. We fitted the low-temperature (below 14 K) heat capacity data to the equation $C_p(T) = \gamma T + \alpha T^{\frac{3}{2}} + \beta T^3$, where electronic ($\gamma T$), ferromagnetic ($\alpha T^{\frac{3}{2}}$) and phonon ($\beta T^3$) contributions are taken into account. We do not get any significant contribution from the magnetic part: the almost linear behaviour of the C_p/T versus T^2 plot (inset of figure 4(a)) indicates the negligible presence of the $\alpha T^{\frac{3}{2}}$ term at low temperature. From the C_p/T versus T^2 data below 14 K, we determine the value of the Debye temperature (Θ_D), and it turns out to be 270 K for the orthorhombic martensite phase. The Sommerfeld

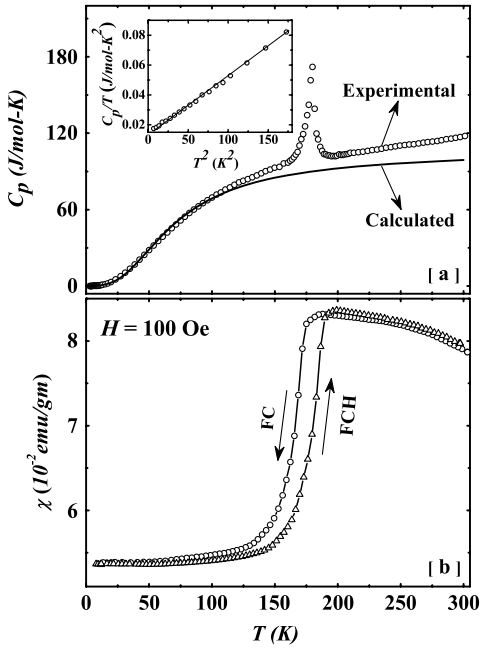

Figure 4. (a) Zero-field heat capacity (C_p) of $Ni_2Mn_{1.4}Sb_{0.6}$ as a function of temperature. The solid line in the curve is the total heat capacity generated by using the low-temperature Θ_D, γ and α (see the discussion in the text). The inset shows the low-temperature C_p/T versus T^2 plot with a linear fit (solid line) to the data. (b) Field-cooling (FC) and field-cooled heating (FCH) magnetic susceptibilities at 100 Oe of applied field.

coefficient (γ) is found to be 13 mJ mol^{-1} K^{-2}. For a comparison, in the case of the full Heusler compound Ni_2MnSb, Θ_D and γ are 222 K and 3.4 mJ mol^{-1} K^{-2}, respectively, as estimated from low-temperature heat capacity data [9]. This stoichiometric Heusler compound does not show an MT and retains its $L2_1$ structure down to low temperatures. We have performed high-T extrapolation of C_p with the full Debye integral by using the parameters obtained from the low-temperature fitting (solid line in figure 4(a)). The extrapolated values start to deviate from the experimental data above 100 K. A T-independent Θ_D is often unsuitable for the whole range of temperature even for a normal crystalline solid. However, looking at the extent and nature of the deviation, presumably it reflects the formation of the high-temperature austenitic phase in the matrix of martensite with a different Θ_D. Although thermal hysteresis in the resistivity data occurs above 135 K, the indication of phase coexistence just above 100 K is quite clear in the magnetic susceptibility and XRD investigations. Interestingly, the value of C_p slightly exceeds the classical Dulong–Petit value of $3pR$ (p = number of atoms per formula unit, R is the ideal gas constant) above the MT. This is presumably due to the enhanced magnetic contribution to the heat capacity close to the second-order phase transition, which was reported to occur just above room temperature [4].

3.4. Magnetization

The temperature dependence of the magnetic susceptibility ($\chi = M/H$) is shown in figure 4(b) for both field-cooled heating (FCH) and field-cooling (FC) conditions. For the FC data, χ shows a sharp drop around 175 K, while in the FCH data, the corresponding sharp rise

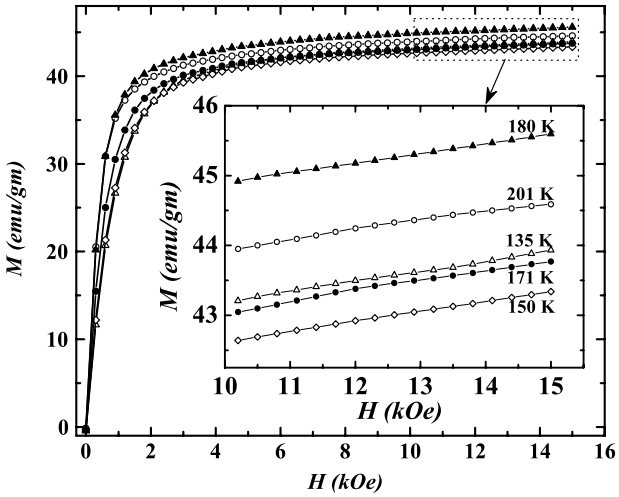

Figure 5. Magnetization as a function of applied field at different temperatures for $Ni_2Mn_{1.4}Sb_{0.6}$. The inset shows an enlarged view of the data.

is observed around 145 K, indicating clear thermal hysteresis due to the MT. The thermal hysteresis extends in the temperature range 75–210 K. Beyond this region of thermal hysteresis, both FC and FCH susceptibilities are almost independent of T, which is in line with the FM nature of the sample. Although the sample is FM throughout the T range of measurement, it is clear from the data that the magnetic moment in the martensite phase is less than that in the austenite phase.

In order to understand the effect of magnetic field on the MT, we carefully recorded isothermal magnetization data as a function of field around the region of metastability (see figure 5). The FM nature of the sample is evident from the nature of these isothermal magnetization curves, as they tend to saturate within 5 kOe of applied field. The saturation fields are found to be a bit higher at low temperatures (below the MT), which is possibly related to the large magneto-crystalline anisotropy in the martensite phase. The saturation magnetization (M_{sat}) at the lowest T of measurement (5 K) was found to be 2.16 μ_B/formula unit. This is comparable to the observed moment of 2.14 μ_B/formula unit for the isostructural compound $Ni_2Mn_{1.44}Sn_{0.56}$ [6]. However, this moment is much smaller as compared to the value obtained (3.7 μ_B/formula unit, at 4.2 K) for the full Heusler compound Ni_2MnSb [10]. Now, if we carefully look at the M–H curves in a restricted temperature window (150–180 K) around the MT, a decrease in M_{sat} is observed as T is lowered. M_{sat}, however, shows its usual trend outside this window, where it increases with decreasing T. This is more clearly visible from the convoluted M–T curves shown in figure 6(a). We have also calculated the change in magnetic entropy due to the application of magnetic field around MT by using the Maxwell's relation:

$$\Delta S(0 \rightarrow H) = \int_0^H \left(\frac{\partial M}{\partial T}\right)_H \mathrm{d}H. \tag{1}$$

This entropy change is related to the adiabatic change in T upon application of H, popularly known as the magneto-caloric effect(MCE) [11]. For this calculation, M versus T data at different constant H were obtained from the isothermal $M(H)$ data recorded at different temperatures (see figure 6(a)). It is clearly seen that the step-like behaviour in $M(T)$ close to the martensitic transition gradually gets suppressed with the increasing field strength. The

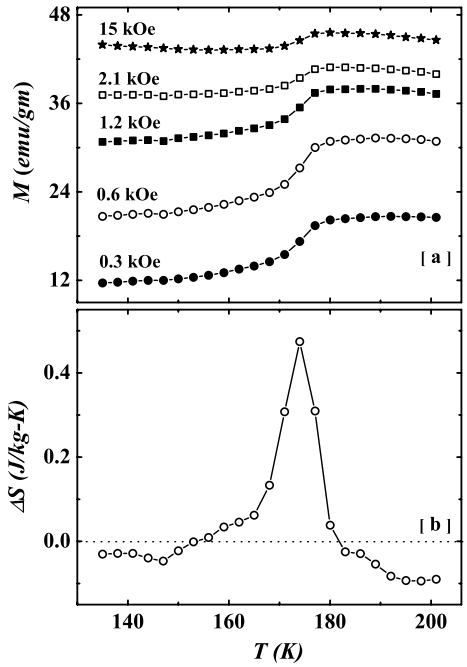

Figure 6. (a) Magnetization versus temperature curves for different applied fields, (b) field-induced entropy change as a function of temperature for applied field H changing from 0 $\rightarrow$ 15 kOe in $Ni_2Mn_{1.4}Sb_{0.6}$.

computed magnetic entropy change (ΔS) is plotted in figure 6(b) as a function of T for change of magnetic field from 0 to 15 kOe. It is evident that ΔS shows a peak close to the MT, which is very similar to the entropy change in magnetic systems near a structural instability [12–14]. However, the magnitude of ΔS is small ($\sim$0.5 J mol^{-1} kg^{-1}) as compared to the reported 2–3 J mol^{-1} kg^{-1} in Ni–Mn–Sn alloys for the similar range of applied field [13]. We observe a positive entropy change ($\Delta S > 0$) for the applied field near the MT for the present compound of investigation. ΔS is however negative outside the region of the MT.

4. Discussion

The present investigation focuses the magnetic and structural behaviour of the shape memory alloy with composition $Ni_2Mn_{1.4}Sb_{0.6}$. The structural instability due to the first-order martensitic transition is associated with a wide region of metastability, where both the austenite and martensite can coexist. This region is characterized by thermal hysteresis in magnetization, resistivity and XRD data. The C_p versus T data show a peak around 179 K, where the majority of the entropy is released. However from our analysis of the heat capacity data, we observe that the anomaly due to the MT is spread over a wide range of T, and the austenite phase starts to develop at temperatures as low as 100 K while heating. This large temperature width of the MT and the phenomenon of phase coexistence are the outcome of a disordered influenced first-order phase transition [7]. Transition-metal-based shape memory alloys are often inherently disordered systems. The influence of disorder on the first-order transition is a well-studied phenomenon [15]. The growth of the product phase in the matrix of the parent phase occurs through nucleation around a defect/disorder. As a result both phases can

coexist and a highly metastable region is developed across the first-order transition temperature. Secondly, the martensitic transition temperature, M_s, is extremely sensitive to the composition in these alloys [4], and a small spatial variation of the composition can give rise to a distribution of M_s. This gives rise to a finite temperature window for the transition.

There are also other interesting features observed in our investigations.

- The region of thermal hysteresis is larger in $\chi(T)$ as compared to the transport data. This is possibly due to the percolation-limited nature of the electronic conduction in a system containing two phases with unequal resistivity. The martensite has a higher resistivity than austenite. While heating from low temperature, until the austenite phase fraction crosses the percolation threshold, the resistivity remains insensitive to the development of the austenite phase. A similar phenomenon happens when the sample is cooled from austenite to martensite. On the other hand, $\chi(T)$ directly measures the magnetization of the sample, and the development of a second phase with different magnetization value is immediately sensed.
- The saturation magnetization of this alloy at low temperature (5 K) is also found to be less (almost half) than the magnetization of the stoichiometric full Heusler system Ni_2MnSb. The stoichiometric compound does not show an MT, and it has a cubic structure at 5 K, whereas $Ni_2Mn_{1.4}Sb_{0.6}$ has an orthorhombic martensitic phase. This discrepancy might be related to the lower value of M in the orthorhombic phase. Secondly, in case of Ni_2MnSb, the magnetic moment comes from localized 3d state of Mn through a hybridization with the p level of Sb [10, 16, 17]. Ni does not contribute to the magnetic moment of the system. The deficiency of Sb in the sample can hinder the full localization of the Mn moment, leading to the reduced value of M_{sat}.
- We also observe a non-monotonic evolution of M_{sat} as a function of T for the sample. Naively, the decrease of M_{sat} around the MT can be assigned to the lower value of M in the martensite. However, one should bear in mind that the sample remains in a region of mixed phase around MT. Since martensite and austenite differ magnetically, the evolution of M_{sat} with respect to T might be complex here.
- A small but positive change in the magnetic entropy under an applied magnetic field near the MT is observed. In case of a ferromagnet, an applied magnetic field helps to increase the magnetic order and we observe a negative change in entropy. The positive entropy change, often termed an inverse magneto-caloric effect (IMCE), is recently seen in some FSMAs, like Ni–Mn–Sn [13], Ni–Mn–Ga [14], Ni–Mn–In [18, 19]. Notably, for $Ni_2Mn_{1.4}Sb_{0.6}$, the IMCE is only observed around the MT (155–180 K); outside this region we observe the usual MCE with $\Delta S < 0$. Considering the fact that the IMCE is only observed in the metastable mixed phase region, it can be attributed to the phenomenon of a field-induced MT. An applied magnetic field, in a system containing both martensite and austenite, can favour the growth of a particular phase by triggering the structural transition. This will change the ratio of the martensite and austenite phase fractions. The magnetic character of FSMAs strongly depends upon the crystal structure, and the field-induced MT will obviously affect the magnetic entropy of the system as well. Recently, a field-induced MT has been observed in Ni–Mn–Sn [5] and Ni–Mn–In alloys [19] by diffraction experiments in the presence of a magnetic field.
- The structural changes due to the MT in the Sb-based alloy $Ni_2Mn_{1.4}Sb_{0.6}$ and in the case of the similar Sn alloy, as probed by the x-ray powder diffraction, are found to be very similar. Both of them assume an 4O orthorhombic phase at low temperatures. This is possibly due to the similar atomic radii of Sn and Sb. The T dependence of M across the MT is also comparable, with a step-like anomaly in $M(T)$ for both Sn and Sb samples. Although both

Sn and Sb samples show an IMCE near the MT, a very small value of ΔS is observed for the present Sb compound as compared to the large change in entropy in $Ni_2Mn_{1.4}Sn_{0.6}$. The small value of ΔS signifies that the observed MT in the present $Ni_2Mn_{1.4}Sb_{0.6}$ alloy is *less sensitive to the applied magnetic field* as compared to its counterparts in Ni–Mn–Sn or Ni–Mn–In systems. The difference in electronic configuration for the Sb alloy can play a role here.

In conclusion, we observe an interesting scenario of a disorder-influenced first-order phase transition in the case of Ni–Mn–Sb shape memory alloy. The first-order transition is smeared over a region of phase coexistence, as seen in various physical properties. A positive albeit small change in entropy under an applied magnetic field signifies a connection between the magnetic and structural aspects of the sample.

Acknowledgments

We thank staff of the high-resolution x-ray diffraction facility (Project No. SP/I2/PU-02/2000, DST) and Unit on Nanoscience and Technology of IACS for helping us in various measurements.

References

[1] Enkovaara J, Ayuela A, Zayak A T, Entel P, Nordstrom L, Dubee M, Jalkanen J, Impola J and Nieminen R M 2004 *Mater. Sci. Eng.* A **378** 52
[2] Sozinov A, Likhachev A A, Lanska N and Ullakko K 2002 *Appl. Phys. Lett.* **80** 1746
[3] Guenin G 1998 *Phase Transit.* **14** 165
[4] Suto Y, Imano Y, Koeda N, Omori T, Kainuma R, Ishida K and Oikawa K 2004 *Appl. Phys. Lett.* **85** 4358
[5] Koyamaa K, Watanabe K, Kanomata T, Kainuma R, Oikawa K and Ishida K 2006 *Appl. Phys. Lett.* **88** 132505
[6] Brown P J, Gandy A P, Ishida K, Kainuma R, Kanomata T, Neumann K U, Oikawa K, Oulanddiaf B and Ziebeck K R A 2006 *J. Phys.: Condens. Matter* **18** 2249
[7] See for a review Roy S B and Chaddah P 2004 *Phase Transit.* **77** 767
[8] Wolter A U B, Bosse A, Baabe D, Maksimov I, Mienert D, Klauß H H, Litterst F J, Niemeier D, Michalak R, Geibel C, Feyerherm R, Hendrikx R, Mydosh J A and Süllow S 2002 *Phys. Rev.* B **66** 174428
[9] Podgornykh S M, Streltsov S V, Kazantsev V A and Shreder E I 2007 *J. Magn. Magn. Mater.* **311** 530
[10] Hurd C M and McAlister S P 1986 *J. Magn. Magn. Mater.* **61** 114
[11] Pecharsky V K and Gschneidner K A Jr 1999 *J. Magn. Magn. Mater.* **200** 44
[12] Zhang Y Q and Zhang Z D 2004 *J. Alloys Compounds* **365** 35
[13] Krenke T, Duman E, Acet M, Wassermann E F, Moya X, Mañosa L and Planes A 2005 *Nat. Mater.* **4** 450
[14] Marcos J, Planes A, Mañosa L, Casanova F, Batlle X, Labarta A and Martínez B 2002 *Phys. Rev.* B **66** 224413
[15] Kartha S, Krumhansl J A, Sethna J P and Wickham L K 1995 *Phys. Rev.* B **52** 803
[16] Kubler J, William A R and Sommers C B 1983 *Phys. Rev.* B **28** 1745
[17] Uhl E 1982 *J. Solid State Chem.* **43** 354
[18] Han Z D, Wang D H, Zhang C L, Tang S L, Gu B X and Du Y W 2006 *Appl. Phys. Lett.* **89** 182507
[19] Krenke T, Duman E, Acet M, Wassermann E F, Moya X, Mañosa L, Planes A, Suard E and Ouladdiaf B 2007 *Phys. Rev.* B **75** 104414